Comparison of Molecular Conductance between Planar and Twisted 4-Phenylpyridines by Means of Two-Dimensional Phase Separation of Tetraphenylporphyrin Templates at a Liquid−HOPG Interface

Takeshi Sakano, Kenji Higashiguchi and Kenji Matsuda*

Received (in XXX, XXX) Xth XXXXXXXXX 200X, Accepted Xth XXXXXXXXX 200X
First published on the web Xth XXXXXXXXX 200X
DOI: 10.1039/b000000x

Tetraphenylporphyrin (TPP) rhodium chlorides coordinated by planar and twisted 4-phenylpyridine derivatives were synthesized. STM image was taken by 2-D phase separation technique and the conductance was evaluated. Difference in apparent height between these phenylpyridines reflects the conductance ratio of ligands.

The investigation of single molecular conductance is a key issue in the molecular electronics field and developing rapidly using several measurement techniques.[1] Although most experiments of the conductance of a single molecule exhibit considerable variations, the reliability of the measurements has recently been significantly increased owing to the statistical treatment by the methods of mechanically controllable break junction (MCBJ)[2] and scanning tunneling microscopy break junction (STM−BJ).[3,4]

Among several methods for the measurement of the molecular conductance, apparent height measurement by STM has the merit of applicability for many samples.[5,6] The method often utilizes the plating of target molecules into the self-assembled monolayers (SAMs) of alkanethiols on Au substrate in order to prevent the intermolecular interaction among target molecules. However, this usual method precludes the statistical treatment because only few spots of target molecules are observable from one STM image. Use of a molecular template is one candidate to avoid the intermolecular interaction and STM observation of the SAM of samples on the templates makes the statistical analysis possible. Herein, we report on the comparison of molecular conductance between planer and twisted 4-phenylpyridine derivatives by using porphyrin templates, and show that two-dimensional (2-D) phase separation technique is effective to discriminate these phenylpyridines on the substrate.

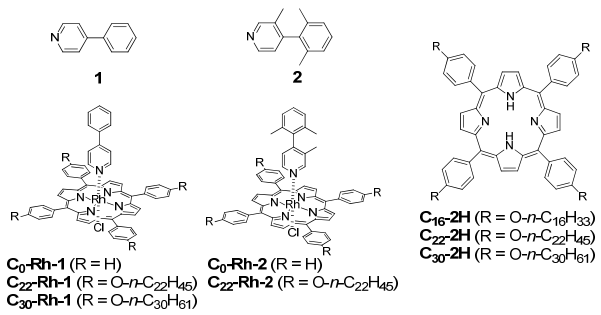

Fig. 1 Molecular structures of synthesized 4-phenylpyridines, TPPs, and TPP rhodium chlorides.

Pyridine-coordinated tetraphenylporphyrin (TPP) Rh(III) chloride having long alkyl chains forms 2-D lamellar structures at a liquid−HOPG interface, where strongly bound axial ligand of pyridine is placed perpendicular on the TPP.[7] Therefore, TPP rhodium chloride can be used as a molecular template for the compounds carrying pyridyl groups. 4-Phenylpyridine derivatives **1** and **2** having the same molecular lengths and the different torsion angles were selected to investigate the differences in the apparent height in STM images because they are expected to have different molecular conductances due to the different torsion angles (Fig. 1).[4]

Syntheses of 4-phenylpyridine-coordinated TPP rhodium chlorides (**C_0-Rh-1**, **C_0-Rh-2**, **C_{22}-Rh-1**, **C_{22}-Rh-2**, and **C_{30}-Rh-1**) were carried out according to the general organic synthesis procedure described in Supplementary Information. Subscript numbers of 0, 22, and 30 show the length of alkyl side chains. Free base TPPs **C_{16}-2H**, **C_{22}-2H**, and **C_{30}-2H** were also synthesized. X-ray crystallographic analysis of **C_0-Rh-1** and **C_0-Rh-2** revealed the dihedral angles between the phenyl ring and the pyridyl ring of **1** and **2** are 27° and 68°, respectively. The ORTEP drawings are shown in Supplementary Information.

STM images for a solution of **C_{22}-Rh-1** and for a 1:1 mixed solution of **C_{22}-Rh-1** and **C_{22}-Rh-2** were obtained at the 1-octanoic acid−HOPG interface in the constant current mode.[8] As shown in Figs. 2a and 2b, both samples formed SAMs of characteristic lamellar structures, where TPPs are aligned side by side in the bright stripes. The stripes are separated by the alkyl chains from the neighboring TPP arrays.[9] In the dark areas the alkyl chains are interdigitated, although detailed structure of these chains was not observed in these images. The lattice parameters of the unit cell $a \times b$ and α were 3.9 ± 0.2 nm × 1.8 ± 0.2 nm and 71° for **C_{22}-Rh-1** and 4.2 ± 0.2 nm × 2.3 ± 0.2 nm and 82° for a mixture of **C_{22}-Rh-1** and **C_{22}-Rh-2**. These values are similar to that of characteristic lamellar structures of **C_{22}-2H** at the phenyloctane–HOPG interface (Fig. S3, ESI†, 4.1 ± 0.2 nm × 1.9 ± 0.2 nm and 84°; also reported in lit.[10] as 4.2 nm × 2.1 nm and 84°).

Contrast of the TPP core shows the apparent height of the core above the alkyl side chains. Section analysis of Fig. 2a is shown in Fig. 2c. Statistical analyses of apparent height for these STM images based on the section analysis are shown in Figs. 2d and 2e. Both statistical distributions of apparent heights were fitted by single Gaussian function. By mixing of **C_{22}-Rh-2** into **C_{22}-Rh-1**, an apparent height distribution got

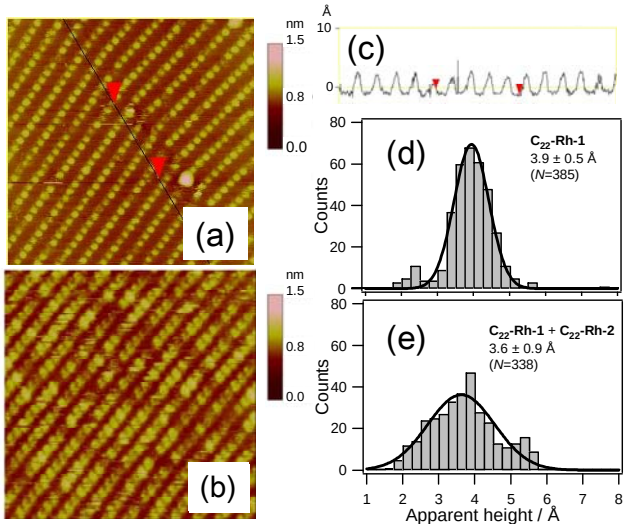

Fig. 2 STM images at the 1-octanoic acid−HOPG interface in the constant current mode: (a) **C_{22}-Rh-1** (3.0×10^{-6} M) (50×50 nm^2, I_{set} = 30 pA, V_{bias} = −1.0 V); (b) a 1:1 mixed solution of **C_{22}-Rh-1** (1.5×10^{-6} M) and **C_{22}-Rh-2** (1.5×10^{-6} M) (60×60 nm^2, I_{set} = 30 pA, V_{bias} = −1.0 V). (c) Section analysis for the image (a). Histograms of apparent height of TPP cores: (d) for the image (a); (e) for the image (b).

lower and broadened from 3.9 ± 0.5 Å to 3.6 ± 0.9 Å. In terms of apparent height, absolute values of the height are generally varied with measurement condition even in the same setup. Therefore, the decrease of apparent height by mixing **C_{22}-Rh-2** does not give the relationship about apparent height between **C_{22}-Rh-1** and **C_{22}-Rh-2**. However, the result of broadening of the distribution suggests that **C_{22}-Rh-2** shows the different apparent height from **C_{22}-Rh-1**. Since topographic heights are the same for **C_{22}-Rh-1** and **C_{22}-Rh-2** at the 1-octanoic acid−HOPG interface, this difference of apparent height shows the difference in tunneling decay constant of axial ligands of **1** and **2**.

To clear up this difference, apparent height distributions for these two ligands need to be distinctly separated. We focused attention on the coadsorption phenomena at a liquid−solid interface[11] and the coadsorption behavior of two free base TPPs, **C_{16}-2H**, **C_{22}-2H**, was examined. Fig. 3a shows STM images for a mixed solution of **C_{16}-2H** and **C_{22}-2H**. Two domains were observed and each domain has different lattice parameters. Lattice parameters of the right domain were 3.4 ± 0.2 nm × 1.8 ± 0.2 nm and 89°, whereas those of left one were 4.0 ± 0.2 nm × 1.6 ± 0.2 nm and 88°. These two parameters are similar to those of **C_{16}-2H** and **C_{22}-2H**. This result shows that the 2-D phase separation of **C_{16}-2H** and **C_{22}-2H** occurred at the solid-liquid interface. Section analysis of each domain shows that there is no significant difference in the apparent height, suggesting that the length of alkyl side chain does not influence the apparent height (Fig. 3b).

By means of the 2-D phase separation method, the apparent height of **1** and **2** were measured. Fig. 4a shows an STM image of a mixed solution of **C_{30}-Rh-1** and **C_{22}-Rh-2**. Two domains having different lattice parameters of unit cell were

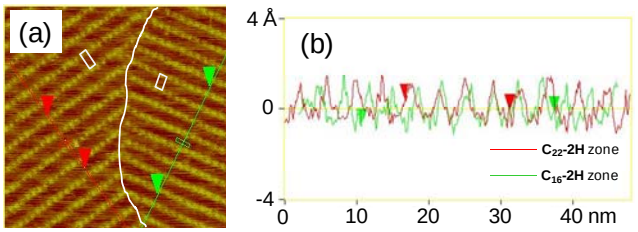

Fig. 3 STM image at the 1-phenyloctane−HOPG interface in the constant current mode: (a) a 3:1 mixed solution of **C_{16}-2H** (1.2×10^{-6}M) and **C_{22}-2H** (4.0×10^{-7}M) (50×50 nm^2, I_{set} = 30 pA, V_{bias} = −1.0 V). (b) Section analyses of **C_{22}-2H** (red line) and **C_{16}-2H** (green line) domains. White parallelograms in the STM images show the unit cells.

observed in one STM image. A domain on the bottom-left corner had a lattice spacing corresponding to that of **C_{30}-2H** (Fig. S3, ESI†) and another one on the upper-right corner had a similar spacing of **C_{22}-2H** lattice. These domains correspond to the domains of **C_{30}-Rh-1** and **C_{22}-Rh-2**. Histograms of apparent height were separately created for each domain as shown in Figs. 4b and 4c. Apparent heights were obtained as 4.3 ± 0.7 Å for **C_{30}-Rh-1** and 2.9 ± 0.6 Å for **C_{22}-Rh-2**. Since geometrical molecular heights of **C_{30}-Rh-1** and **C_{22}-Rh-2** are the same, the difference of apparent height should originate from the conductance ratio of two ligands **1** and **2**. Summation of these histograms gave a broad distribution (Fig. 4d), which is in good agreement with the distribution of an apparent height of 1:1 mixture of **C_{22}-Rh-1** and **C_{22}-Rh-2** that has already been shown in Fig. 2e.

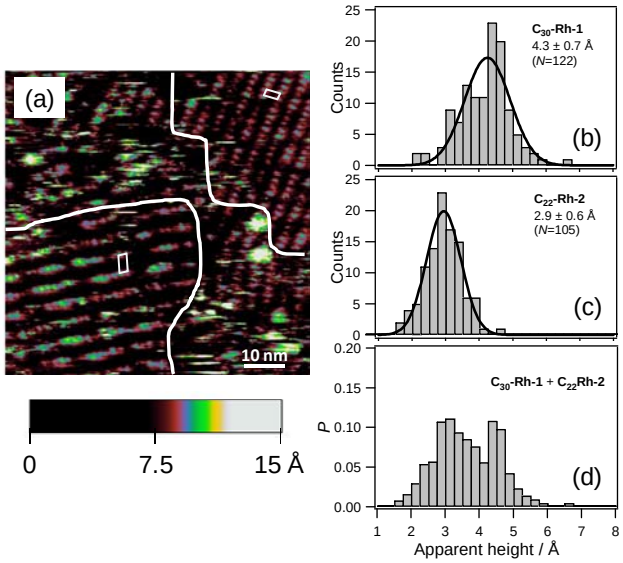

Fig. 4 (a) An STM image of a 10:1 mixed solution of **C_{22}-Rh-2** (1.5×10^{-6} M) and **C_{30}-Rh-1** (1.5×10^{-7} M) (75×75 nm^2, I_{set} = 30 pA, V_{bias} = −1.0 V) at the 1-octanoic acid−HOPG interface in the constant current mode. Histograms of apparent height in the domain of (b) **C_{30}-Rh-1**, (c) **C_{22}-Rh-2**, and (d) both **C_{30}-Rh-1** and **C_{22}-Rh-2**. The contribution in counts from each domain was normalized to 1:1 in histogram (d).

According to the two-layer tunnel junction model proposed by Weiss et al,[5] the total conductance (G_{total}) between an STM tip and a substrate is described by product of the gap conductance ($G_{gap} = A \exp(-\alpha d)$) and molecular conductance ($G_{mol} = B \exp(-\beta x)$), where A and B are contact conductances,

α and β are decay constants of the gap and the molecule, d is gap distance and x is molecular length. G_{total} is constant everywhere, therefore, conductance ratio (G_{mol1}/G_{mol2}) is given by the following equation 1:

$$\frac{G_{mol1}}{G_{mol2}} = \frac{G_{gap2}}{G_{gap1}} = \frac{A_2}{A_1}\exp\{\alpha(d_1 - d_2)\} \quad (1)$$

This equation means that the ratio of A_2/A_1, decay constant of the gap (α), and difference of gap distance ($d_1 - d_2$) give the conductance ratio. The measurement condition is identical because STM measurement was carried out for structurally similar phenylpyridines **C_{30}-Rh-1** and **C_{22}-Rh-2** and the both molecules were observed in the same STM image. Therefore, contact-dependent terms A_1 and A_2 are assumed to be equal. Additionally, because x_1 and x_2 are the same, the term ($d_1 - d_2$) is equal to the difference of apparent height Δh_{STM} (Fig. 5). Then, equation 1 is transformed to the following simple form:

$$\frac{G_{mol1}}{G_{mol2}} = \exp\{\alpha \Delta h_{STM}\} \quad (2)$$

This equation 2 means that decay constant α of the gap and experimentally obtained Δh_{STM} gives the conductance ratio between **C_{30}-Rh-1** and **C_{22}-Rh-2**. Since the STM measurement was conducted at the 1-octanoic acid−HOPG interface, α value of vacuum can not be applied. We adopted the decay constant of methylene unit ($\beta = 1.2$ Å^{-1}) reported by the measurement of a series of alkanethiols as a substitute of 1-octanoic acid.[5] By introducing the measurement result Δh_{STM} = 1.4 Å, the conductance ratio between **C_{30}-Rh-1** and **C_{22}-Rh-2** is finally obtained to be G_{mol1}/G_{mol2} = 5.4. Since these phenylpyridines **1** and **2** are supported by cognate templates, this conductance ratio originated from the twisting effect of the ligands. This result was compared to $\cos^2\phi$ law proposed by Venkataraman et al., in which molecular conductance of 4,4′-diaminobiphenyl is proportional to the $\cos^2\phi$, where ϕ is a dihedral angle.[4] Dihedral angles of **1** (27°) and **2** (68°) obtained from X-ray crystallographic analysis give conductance ratio $\cos^2\phi_1/\cos^2\phi_2$ = 5.7, which is in excellent agreement with experimentally obtained G_{mol1}/G_{mol2} = 5.4. This agreement warrants that our method is applicable to the comparison of molecular conductance.

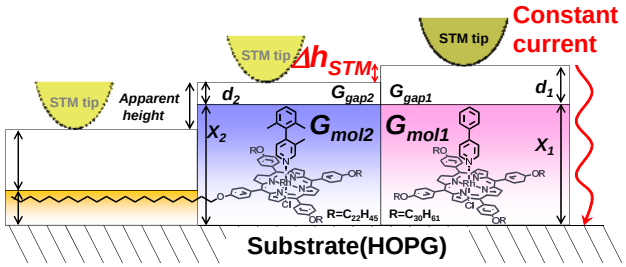

Fig 5 Schematic drawing of the two-layer tunnel junction model for the STM measurement of a mixed solution of **C_{30}-Rh-1** and **C_{22}-Rh-2**.

In conclusion, we have succeeded to develop the 2-D phase separation technique of TPP templates having different lengths of side chain at a solution–HOPG interface. This technique was applied to the determination of the ratio of molecular conductance between planar and twisted phenylpyridines by comparing apparent height in the STM image. This technique will be the useful method for the determination of molecular conductance.

This work was supported by a Grant-in-Aid for Young Scientist (A) (No. 19685013) and a Grant-in-Aid for Science Research in Priority Areas "Photochromism (471)" (No. 19050009) from MEXT, Japan and NEXT program (No. GR062) from JSPS, Japan. T. S. acknowledges JSPS for the young scientist fellowship.

Notes and references

Department of Synthetic Chemistry and Biological Chemistry, Graduate School of Engineering, Kyoto University, Katsura, Nishikyo-ku, Kyoto 615-8510, Japan; E-mail: kmatsuda@sbchem.kyoto-u.ac.jp

† Electronic Supplementary Information (ESI) available: Synthetic procedures of a 4-phenylpyridine derivative, TPP rhodium chlorides, ^{1}H NMR spectra of all compounds, additional STM images, details of lattice parameters, and crystallographic data of **C_0-Rh-1** and **C_0-Rh-2**. CCDC 814313-4. See DOI: 10.1039/b000000x/

1 C. Joachim, J. K. Gimzewski, A. Aviram, *Nature*, 2000, **408**, 541–548.; A. Nitzan, M. A. Ratner, *Science*, 2003, **300**, 1384-1389.; A. Salomon, D. Cahen, S. Lindsay, J. Tomfohr, V. B. Engelkes, C. D. Frisbie, *Adv. Mater.*, 2003, **15**, 1881-1890.; C. Joachim, M. A. Ratner, *Proc. Natl. Acad. Sci. U.S.A.*, 2005, **102**, 8801-8802.; N. J. Tao, *Nat. Nanotechnol.*, 2006, **1**, 173–181.; P. S. Weiss, *Acc. Chem. Res.*, 2008, **41**, 1772–1781.; K. Moth-Poulsen, T. Bjørnholm, *Nat. Nanotechnol.*, 2009, **4**, 551-556.

2 M. A. Reed, C. Zhou, C. J. Muller, T. P. Burgin, J. M. Tour, *Science*, 1997, **278**, 252–254.; M. T. Gonzalez, S. M. Wu, R. Huber, S. J. van der Molen, C. Schonenberger, M. Calame, *Nano Lett.*, 2006, **6**, 2238–2242.; M. Tsutsui, M. Taniguchi, K. Yokota, T. Kawai, *Nat. Nanotechnol.*, 2010, **5**, 286–290.

3 B. Xu, N. J. Tao, *Science*, 2003, **301**, 1221–1223.

4 L. Venkataraman, J. E. Klare, C. Nuckolls, M. S. Hybertsen, M. L. Steigerwald, *Nature*, 2006, **442**, 904–907.; D. Vonlanthen, A. Mishchenko, M. Elbing, M. Neuburger, T. Wandlowski, M. Mayor, *Angew. Chem. Int. Ed.*, 2009, **48**, 8886–8890.; A. Mishchenko, D. Vonlanthen, V. Meded, M. Bürkle, C. Li, I. V. Pobelov, A. Bagrets, J. K. Viljas, F. Pauly, F. Evers, M. Mayor, T. Wandlowski, *Nano Lett.*, 2010, **10**, 156–163.

5 L. A. Bumm, J. J. Arnold, T. D. Dunbar, D. L. Allara, P. S. Weiss, *J. Phys. Chem. B*, 1999, **103**, 8122–8127.

6 K. Moth-Poulsen, L. Patrone, N. Stuhr-Hansen, J. B. Christensen, J.-P. Bourgoin, T. Bjørnholm, *Nano Lett.*, 2005, **5**, 783–785.; S. Wakamatsu, S. Fujii, U. Akiba, M. Fujihira, *Jpn. J. Appl. Phys.*, 2006, **45**, 2736–2742.

7 J. Otsuki, *Coord. Chem. Rev.* 2010, **254**, 2311-2341.; T. Ikeda, M. Asakawa, M. Goto, K. Miyake, T. Ishida, T. Shimizu, *Langmuir*, 2004, **20**, 5454–5459.

8 UV-vis spectrum of the ligand-coordinated porphyrin in octanoic acid showed 3nm of red-shift compared with the ligand-free porphyrin, suggesting that the pyridyl ligand is bound to the porphyrin template. See M. Hoshino, H. Seki, K. Yasufuku, H. Shizuka, *J. Phys. Chem.* 1986, **90**, 5149-5153.

9 X. Qiu, C. Wang, Q. Zeng, B. Xu, S. Yin, H. Wang, S. Xu, C. Bai, *J. Am. Chem. Soc.*, 2000, **122**, 5550–5556.; H. Wang, C. Wang, Q. Zeng, S. Xu, S. Yin, B. Xu, C. Bai, *Surf. Interface Anal.*, 2001, **32**, 266–270.

10 J. Otsuki, S. Kawaguchi, T. Yamakawa, M. Asakawa, K. Miyake, *Langmuir*, 2006, **22**, 5708–5715.

11 F. Tao, J. Goswami, S. L. Bernasek, *J. Phys. Chem. B*, 2006, **110**, 19562–19569.

Graphical abstract

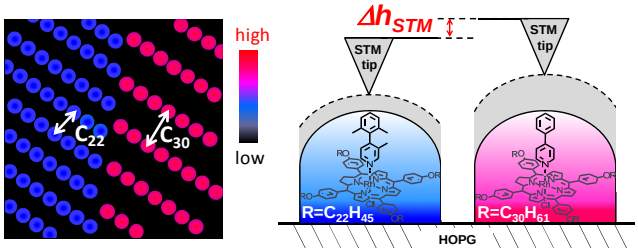

STM image of tetraphenylporphyrins coordinated by phenylpyridine derivatives was taken by 2-D phase separation technique and the conductance was evaluated.